Available online at www.sciencedirect.com
SCIENCE DIRECT
Journal of Catalysis 226 (2004) 292–300
JOURNAL OF CATALYSIS
www.elsevier.com/locate/jcat

Oxidative dehydrogenation of propane over vanadia-based catalysts supported on high-surface-area mesoporous $MgAl_2O_4$

Owen R. Evans, Alexis T. Bell *, T. Don Tilley

Chemical Sciences Division, Lawrence Berkeley National Laboratory, and Department of Chemistry and Chemical Engineering, University of California, Berkeley, CA 94720-1462, USA

Received 12 January 2004; revised 1 June 2004; accepted 2 June 2004

Available online 2 July 2004

Abstract

The oxidative dehydrogenation of propane to propene was investigated over a series of novel vanadia-based catalysts supported on high-surface-area magnesium spinel. A mesoporous $MgAl_2O_4$ support was synthesized via a low-temperature sol–gel process involving the heterobimetallic alkoxide precursor, $Mg[Al(O^iPr)_4]_2$. A high-purity catalyst support was obtained after calcination at 1173 K under O_2 atmosphere and active vanadia catalysts were prepared from the thermolysis of $OV(O^tBu)_3$ after grafting onto the spinel support. $MgAl_2O_4$-supported catalysts prepared in this manner have BET surface areas of 234–245 m^2/g. All of the catalysts were characterized by X-ray powder diffraction, and Raman, solid-state NMR, and diffuse-reflectance UV–vis spectroscopy. At all vanadium loadings the vanadia supported on $MgAl_2O_4$ exist as a combination of isolated monovanadate and tetrahedral polyvanadate species. As the vanadium surface density increases for these catalysts the ratio of polyvanadate species to isolated monovandate species increases. In addition, as the vanadium surface density increases for these catalysts, the initial rate of propane ODH per V atom increases and reaches a maximum value at 6 VO_x/nm^2. Increasing the vanadium surface density past this point results in a decrease in the rate of propane ODH owing to the formation of multilayer species in which subsurface vanadium atoms are essentially rendered catalytically inactive. The initial propene selectivity increases with increasing vanadium surface density and reaches a plateau of $\sim 95\%$ for the V/MgAl catalysts. Rate coefficients for propane ODH (k_1), propane combustion (k_2), and propene combustion (k_3) were calculated for these catalysts. The value of k_1 increases with increasing VO_x surface density, reaching a maximum at about 5.5 VO_x/nm^2. On the other hand, the ratio (k_2/k_1) for V/MgAl decreases with increasing VO_x surface density. The ratio (k_3/k_1) for both sets of catalysts shows no dependence on the vanadia surface density. The observed trends in k_1, (k_2/k_1), and (k_3/k_1) are discussed in terms of the surface structure of the catalyst.

Keywords: Propane; Oxidative dehydrogenation; Vanadia

1. Introduction

The motivation for developing active and selective catalysts that will dehydrogenate propane to propene is the ability to take an inexpensive and abundant alkane feedstock and convert it to a considerably more valuable and synthetically useful olefin. Currently, commercial conversion of propane to propene is based on an endothermic, nonoxidative process using chromium-based catalysts, resulting in H_2 as a by-product. Because this reaction is endothermic, temperatures in excess of 873 K are needed to obtain high propene yields. The thermal dehydrogenation process is energy intensive and because of the temperatures required, catalyst coking and undesired methane formation are inherent problems. Alternatively, oxidative dehydrogenation (ODH) relies on the oxidation of the H_2 by-product to H_2O and thus utilizes the heat of formation of water to turn an otherwise endothermic process into an exothermic one. In theory, ODH processes can be run at lower temperatures that allow for an improvement in selectivity and/or yield of propene. Unfortunately, the addition of oxygen also allows for competing combustion reactions of propane or propene to carbon oxides. These competing reactions lower propene selectivity and have thus far prevented the ODH process from becoming commercially viable. Therefore, current research is focused primarily on the development of an active ODH catalyst exhibiting high olefin selectivity.

* Corresponding author.
E-mail address: bell@cchem.berkeley.edu (A.T. Bell).

0021-9517/$ – see front matter
doi:10.1016/j.jcat.2004.06.002

Recent work has focused on the development of ODH catalysts composed of vanadia supported on metal oxides such as MgO, Al_2O_3, ZrO_2, SiO_2, and TiO_2 [1–12]. The choice of catalyst support plays an important role in the dispersion and electronic properties of the dispersed vanadium species. It has also been shown that the acid–base properties of these supports strongly affect propene selectivity [13–17]. For example, V–Mg–O catalysts show improved propene selectivities compared to catalysts supported on less basic metal oxides [3,4]. We have recently shown that vanadia supported on nanocrystalline MgO is a very selective and active catalyst for the ODH of propane [1]. It is thought that the use of a basic metal oxide support results in improved selectivities because of a rapid desorption of the electron-rich propene product before further combustion to CO_x can result. We have also previously reported that γ-Al_2O_3 is an excellent support for the synthesis of well-dispersed VO_x species that are active and selective in the ODH of propane despite the presence of moderate Lewis acid sites on the support [2]. Recently, Lemonidou and co-workers improved the propene selectivity of VO_x/Al_2O_3 catalysts by 10–17% via the incorporation of 9 wt% MgO [13]. It was found in this case that the catalyst support is a mixture of crystalline MgO and γ-Al_2O_3. Interestingly, temperature-programmed desorption experiments performed on these catalysts revealed a decrease in propene adsorption upon introduction of the MgO modifier. It thus follows that further decreases in propene adsorption and hence improved propene selectivities should result upon introduction of a larger percentage of MgO. Based on the obvious beneficial effect of Mg addition we propose that vanadia catalysts supported on the pure mixed-metal oxide $MgAl_2O_4$ should exhibit improved selectivities in comparison to VO_x/Al_2O_3 and MgO-modified VO_x/Al_2O_3. Herein, we would like to report the development of active and selective vanadia-based ODH catalysts supported on a high-surface-area $MgAl_2O_4$ support.

2. Experimental

High-surface-area $MgAl_2O_4$ was prepared using a modification of a previously reported method [18]. An isopropanol solution (25 ml) of $Mg[Al(O^iPr)_4]_2$ (17 mmol) was cooled to 195 K in a dry-ice/acetone bath. A solution of water (> 8 eq) and isopropanol (10 ml) was added dropwise with vigorous stirring to the reaction mixture. After addition, stirring was discontinued and the reaction mixture was allowed to warm to room temperature. The homogeneous transparent gel obtained was allowed to air-dry in a petri dish for 16 h. Any remaining volatiles were then removed by drying under vacuum at 253 K for 4 h. The xerogel was then calcined for 4 h under O_2 atmosphere at 1173 K.

The vanadium precursor $OV(O^tBu)_3$ was synthesized by reaction of V_2O_5 (Aldrich) with ^{t}BuOH in benzene [19]. The preparation of this compound was carried out in an inert atmosphere using a Schlenk line. Twenty grams of V_2O_5 was first placed in a 1-L round-bottom flask and connected to a Dean–Stark trap to capture the water from the reaction and the reflux condenser. After adding 300-ml of benzene, 165 ml of ^{t}BuOH was added to the benzene suspension of V_2O_5. The temperature was increased to ca. 368 K and maintained overnight. After reaction, the color of the solution changed to orange from red. The solution was filtered away from unreacted V_2O_5. After removal of the solvent by distillation, white crystals were observed. This product was further dried overnight under reduced pressure. To purify the freshly formed product ($OV(O^tBu)_3$), sublimation was conducted under vacuum at 313 K. After purification, the compound was identified by the presence of a strong ^{1}H NMR resonance at 1.44 ppm.

V/MgAl catalysts were prepared by impregnation of $MgAl_2O_4$ with a toluene solution of $OV(O^tBu)_3$. A solution of $OV(O^tBu)_3$ in toluene was added with stirring to a dry sample of $MgAl_2O_4$ in a 100-ml Schlenk roundbottom flask. After 1 h of stirring, the toluene was removed by evaporation under vacuum. Calcination of the catalyst was performed by heating to 823 K at 1 K/min and holding for 6 h in a flow of air. The samples were labeled *n* V/MgAl, where *n* is the nominal weight percentage of V_2O_5 in the sample.

Surface areas were measured by N_2 physisorption using a Quantasorb apparatus (Quantachrome Corporation) and standard multipoint BET analysis methods. Samples were evacuated for 3 h at 383 K before N_2 (Airgas, 99.999%) physisorption measurements. Powder X-ray diffraction patterns were obtained at room temperature using a Siemens diffractometer and Cu-K_α radiation and a small catalyst sample mixed with Vaseline and spread on a thin glass plate. Raman spectra were obtained using a HoloLab Series 5000 Raman spectrometer (Kaiser Optical) equipped with an Nd-YAG laser that is frequency-doubled to 532 nm. Samples (50 mg) were pressed into wafers at 350 MPa pressure (0.9 cm diameter, 0.1 cm thickness) and placed within a quartz cell. The laser was operated at a power level of 75 mW. The sample stage was rotated at 20 Hz in order to reduce the effect of laser heating on the local sample temperature. Raman spectra of hydrated samples were recorded under ambient conditions. Samples were dehydrated at 673 K in 20% O_2/He for 1 h and then cooled to room temperature in the same atmosphere before measurement of Raman spectra. Diffuse reflectance UV–vis (DR–UV–vis) spectra were recorded using a Varian-Cary 4 spectrophotometer equipped with a Harrick diffuse reflectance attachment. MgO was used as a reference. Reflectance measurements were converted to absorption spectra using the Kubelka–Munk function. UV–vis spectra were measured in the range of 1.5–50 eV at room temperature. Samples were dehydrated at 673 K in O_2 for 1 h and then cooled to room temperature in the same atmosphere before measurement of DRUV–vis spectra. Wideline 51V SS-NMR spectra were acquired using the Oldfield echo pulse sequence, 45–τ_1–90–τ_2 with τ_1

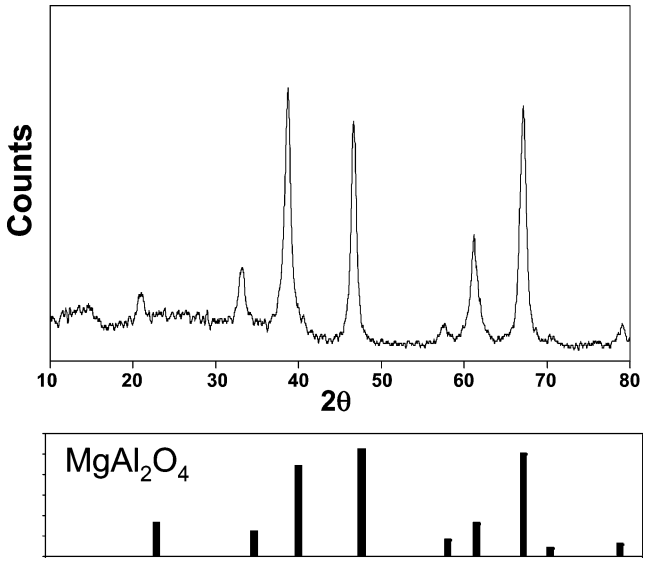

Fig. 1. Powder XRD pattern of the catalyst support, $MgAl_2O_4$. The peaks and relative intensities obtained from JCPDS file 21-1152 are shown at the bottom.

being 30 µs. The dwell time was 0.75 µs, and the pulse delay was 0.5 s.

Rates of reaction and selectivities for the oxidative dehydrogenation of propane were measured in a fixed-bed quartz reactor using 15 mg of catalyst diluted with quartz powder (0.50 g; particle size, 0.246–0.495 mm) to prevent temperature gradients. A mixture of propane (25 cm^3/min), oxygen (9 cm^3/min), and nitrogen (2 cm^3/min) in He (200 cm^3/min) was introduced into the reactor at controlled flow rates. The gaseous reactants and products were analyzed online with a Hewlett–Packard 6890 gas chromatograph equipped with both a capillary column (HP-1) and a packed column (HAYESEP-Q). Only C_3H_6, CO, CO_2, and H_2O were observed as products. The conversion of propane was measured at total flow rates of 60–235 cm^3/min and reaction temperatures of 673, 723, and 773 K.

3. Results and discussion

3.1. Catalyst synthesis and structure

Mesoporous high-purity $MgAl_2O_4$ was obtained in high yield using a sol–gel route involving the low-temperature hydrolysis of the heterobimetallic alkoxide, $Mg[Al(O^iPr)_4]_2$. Fig. 1 shows the powder X-ray diffraction (XRD) pattern of the as-made $MgAl_2O_4$ after calcination at 1173 K (Fig. 1, top). The peaks and intensities of this XRD pattern match that of pure $MgAl_2O_4$ (Fig. 1, bottom). The presence of MgO was not observed. An average $MgAl_2O_4$ particle size of 9.2 nm was estimated from the powder XRD pattern via the Scherrer equation, using the width of the peak at 19.4°. The Brunauer–Emmett–Teller (BET) surface area of the spinel support after calcination to 1173 K in O_2 atmosphere is 300 m^2/g.

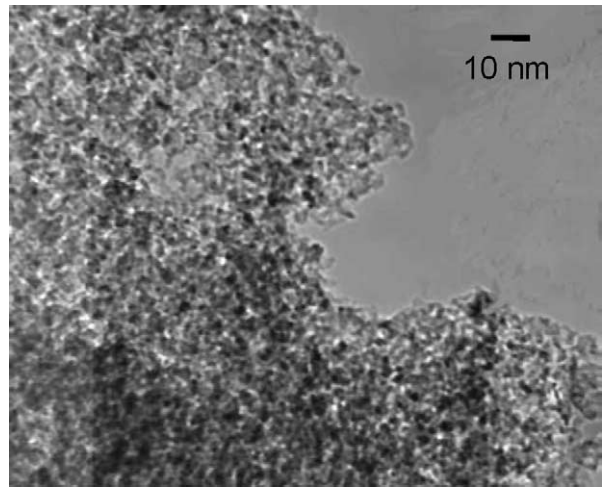

Fig. 2. Transmission electron micrograph of the $MgAl_2O_4$ support.

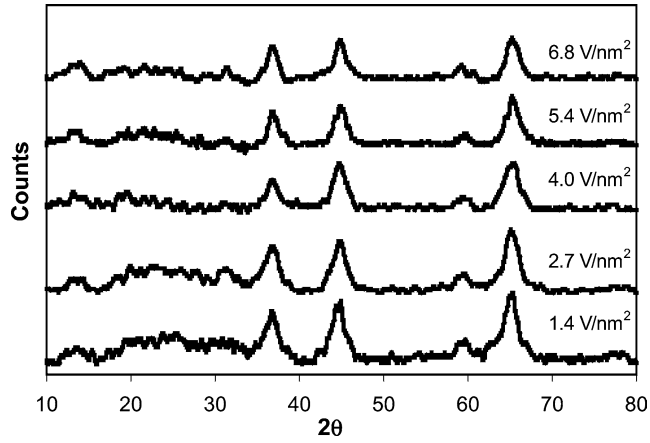

Fig. 3. XRD powder patterns of V/MgAl catalysts as a function of vanadium loading.

To further characterize the morphology of the bare support, it was examined by transmission electron microscopy (TEM). As shown in Fig. 2, the support appears to be composed of aggregates of small particles with diameters of ca. 9 nm, consistent with the average particle size estimated from the powder XRD pattern.

A series of vanadia catalysts were prepared via the nonaqueous grafting of a well-defined molecular precursor, $OV(O^tBu)_3$, onto the surface of the catalyst support. The active form of the catalyst was then obtained via the thermolysis of this precursor. We have shown previously that this grafting procedure leads to a superior dispersion of VO_x species compared to traditional aqueous impregnation methods [1]. Fig. 3 shows the XRD patterns of the V/MgAl catalysts after calcination to 823 K. The only peaks observable are those attributed to the catalyst support and there is no evidence of crystalline V_2O_5. As the vanadia loading increases, the V/MgAl catalysts exhibit a slight decrease in BET surface area and an increase in apparent VO_x surface densities (Table 1). For the 25 V/MgAl catalyst, the apparent VO_x sur-

Table 1
Surface area, nominal loading, apparent surface density of VO_x, and UV–vis absorption edge energy for V/MgAl and V/Al_2O_3catalysts

Sample	Nominal wt% of V_2O_5	Surface area (m^2/g)	Apparent surface density (VO_x/nm^2)[a]	Absorption edge energy (eV)
5 V/MgAl	5	245	1.4	2.89
10 V/MgAl	10	243	2.7	2.91
15 V/MgAl	15	240	4.0	2.92
20 V/MgAl	20	238	5.4	2.88
25 V/MgAl	25	234	6.8	2.82
2 V/Al_2O_3[b]	2	95	1.4	2.73
5 V/Al_2O_3[b]	5	93	3.6	2.68
10 V/Al_2O_3[b]	10	83	8.0	2.29
15 V/Al_2O_3[b]	15	80	12.5	2.09

[a] Assuming all the VO_x is exposed to the surface.
[b] Data obtained from Ref. [2].

face density approaches the value obtained for a theoretical polyvanadate monolayer, 7–8 VO_x/nm^2 [20].

Raman spectra of all the V/MgAl catalysts are shown in Fig. 4. Peaks attributable to bare $MgAl_2O_4$ support were too weak or broadened to be observed. All catalysts exhibit a peak centered at 1035 cm^{-1} which can be assigned to a terminal V=O stretch from surface monovanadate species [21–24]. Broad bands from 910–980 cm^{-1} are evident in all samples and can be tentatively assigned to V=O stretching modes in polyvanadate species [8]. Note that as the vanadia loading increases, the intensity of this band increases relative to that of the isolated monovanadate peak. This behavior suggests that as the vanadia loading increases, the number of isolated monovanadate species decreases at the expense of polyvanadate formation. In comparison to the Raman spectra reported for VO_x/Al_2O_3, the peaks are significantly broadened. The phonon confinement model [25,26] has recently been used to explain the significant Raman peak broadening displayed by particles with diameters in the nanoscale regime (sizes < 50 nm). The Raman peak broadening exhibited by the V/MgAl catalysts is likely the result of a reduced VO_x domain size and thus suggests a very high dispersion of vanadia. None of the V/MgAl catalysts showed evidence for bulk V_2O_5 formation, identified by bands at 405, 489, 524, 694, and 998 cm^{-1}. It can be inferred from the Raman spectra of the V/MgAl catalysts that the VO_x species likely exist as highly dispersed monovanadate and two-dimensional polyvanadate species.

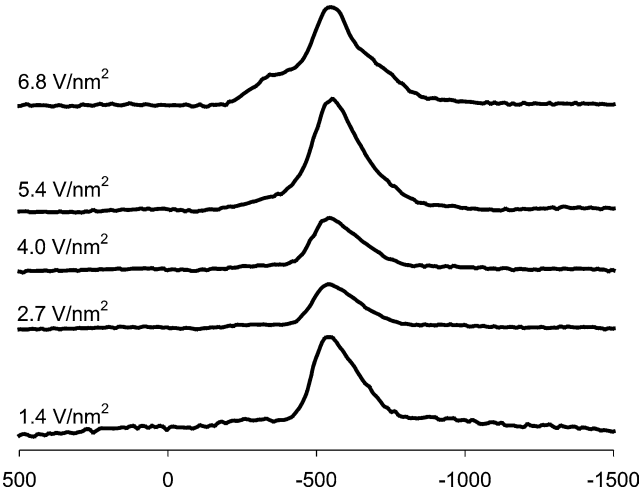

Fig. 5. Static solid-state ^{51}V NMR of the V/MgAl catalysts as a function of vanadium loading.

Static solid-state ^{51}V NMR spectra for V/MgAl catalysts are shown in Fig. 5. At all vanadium weight loadings,

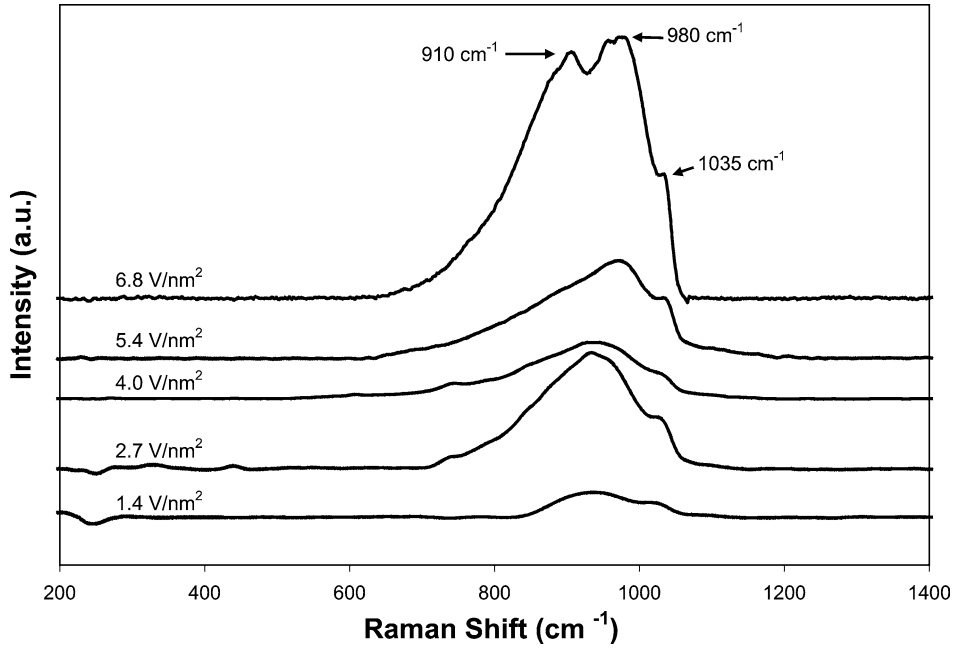

Fig. 4. Raman spectra of the V/MgAl catalysts as a function of vanadium loading.

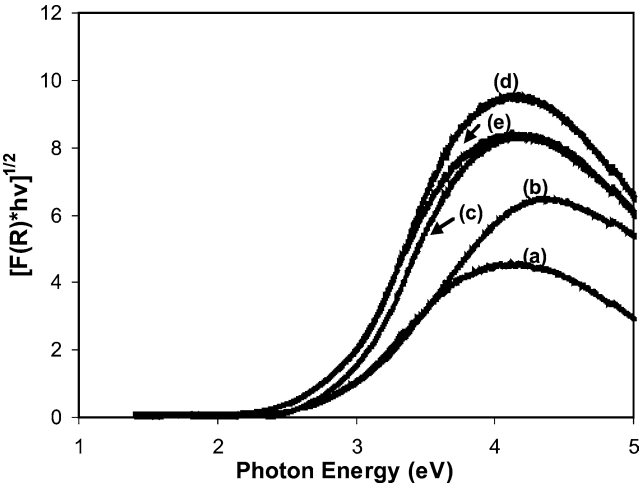

Fig. 6. Diffuse reflectance UV–vis spectra of the V/MgAl catalysts as a function of vanadium loading (V_2O_5 wt%): (a) 5, (b) 10, (c) 15, (d) 20, (e) 25.

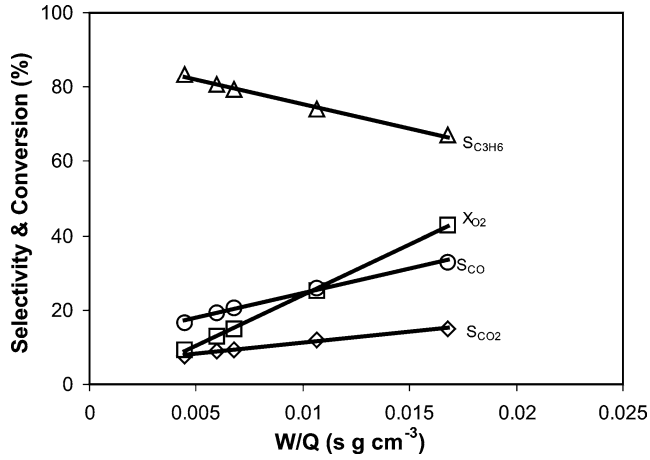

Fig. 7. Product selectivities and oxygen conversions in the oxidative dehydrogenation of propane on the 25 V/MgAl catalyst. Reaction conditions: temperature, 773 K; $C_3H_8/He/O_2$, 25/200/9; total flow rate, 20–220 cm^3/min; pressure, 1 atm; catalyst mass, 0.025 g.

these spectra display one major anisotropic peak centered at −516 ppm, which is attributed to tetrahedral vanadium–oxygen structures [27]. At higher vanadium weight loadings, a small shoulder centered at −350 ppm begins to appear which can be attributed to surface vanadium–oxygen structures surrounded by an octahedron of oxygen atoms. The appearance of this peak occurs at a vanadium surface density of ∼ 6 V/nm^2 and is due to the formation of a polyvanadate monolayer and a greater oligomerization of VO_x surface species. This behavior is consistent with the results obtained from Raman spectroscopy.

Diffuse reflectance UV–vis spectra of the V/MgAl catalysts pretreated at 673 K under O_2 atmosphere are shown in Fig. 6. Absorption bands in the range 2–4 eV arise from O^{2-} to V^{5+} ligand-to-metal charge transfer transitions. Charge transfer bands for the bare $MgAl_2O_4$ support occur at much higher energies and do not obscure the region corresponding to the absorption peak for VO_x-related species. Owing to the broadness of the VO_x absorption bands it is more useful to characterize these charge-transfer transitions by the energy of the absorption edge which is defined as the first inflection point in the Kubelka–Munk function [28]. The absorption edge energies for all catalysts are shown in Table 1. These energies lie within the limits defined by those for the model pseudo-tetrahedral compound $OV[OSi(O^tBu)_3]_3$ (3.95 eV) and V_2O_5 (2.21 eV) where vanadium atoms adopt a distorted octahedral environment. The absorption edge energies for the V/MgAl catalysts decrease with increasing vanadium loading. Studies have shown that absorption edge energies are inversely proportional to the size and dimensionality of VO_x surface species [29]. The DRUV–vis data thus suggest that the decrease in absorption edge energy for the V/MgAl catalysts is consistent with a progression from isolated pseudo-tetrahedral monovandate species to oligomeric VO_x species. This conclusion is also supported with the data obtained from Raman and ^{51}V SS-NMR spectroscopy. The higher absorption edge energies of the V/MgAl catalysts versus those obtained for VO_x/Al_2O_3 (Table 1) suggest an increase in the degree of VO_x dispersion and the existence of smaller two-dimensional polyvanadate domains. This hypothesis is also supported by data obtained from Raman spectroscopy.

3.2. Catalyst activity and selectivity

The effects of bed residence time on O_2 conversion and on C_3H_6, CO, and CO_2 selectivities for 25 V/MgAl at 773 K are shown in Fig. 7. The selectivity to propene steadily decreases with increasing propene conversion as a consequence of increasing combustion of propene [30]. Consistent with this interpretation, the selectivity to CO and CO_2 increases with increasing propane conversion. Interestingly, the selectivity to CO is considerably higher than the selectivity to CO_2. It has been shown that the production of CO is mainly a consequence of the secondary combustion of propene, whereas CO_2 stems mainly from the primary combustion of propane [5,31–33].

The rate of propene formation at zero residence time normalized per V atom, is shown in Fig. 8 as a function of vanadia surface density for all V/MgAl catalysts. In general, the propene activity increases dramatically with increasing vanadium surface densities and appears to plateau at a vanadium surface density of ∼ 6 V/nm^2. This trend of activity as a function of vanadium surface density is similar to that reported for VO_x/Al_2O_3 except that the activities decrease past a vanadium surface density of 6 V/nm^2. This decrease of activity beyond 6 V/nm^2 can be ascribed to the formation of vanadia multilayers in which vanadium atoms lying below the surface are rendered catalytically inactive. On the other hand, the plateau in activities for the V/MgAl catalysts suggest that at similar weight loadings, the VO_x species in these catalysts are considerably more dispersed than those found on Al_2O_3. The increase in ODH rate per V atom with increasing vanadium surface density seen for vanadium weight

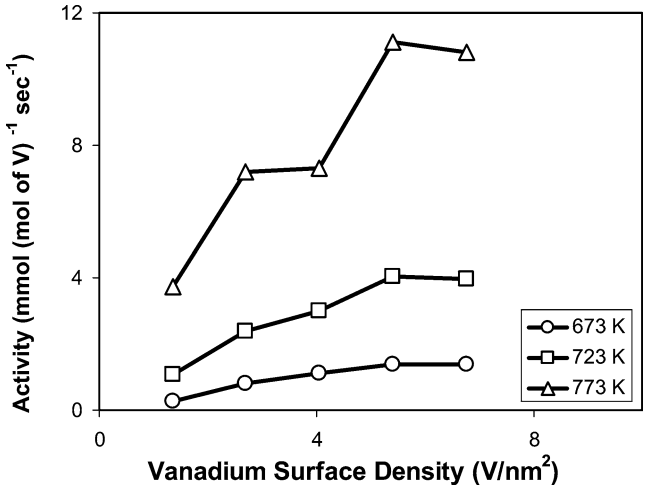

Fig. 8. Effects of apparent surface density and reaction temperatures on the initial rate of propene formation normalized per V atom for the V/MgAl catalysts.

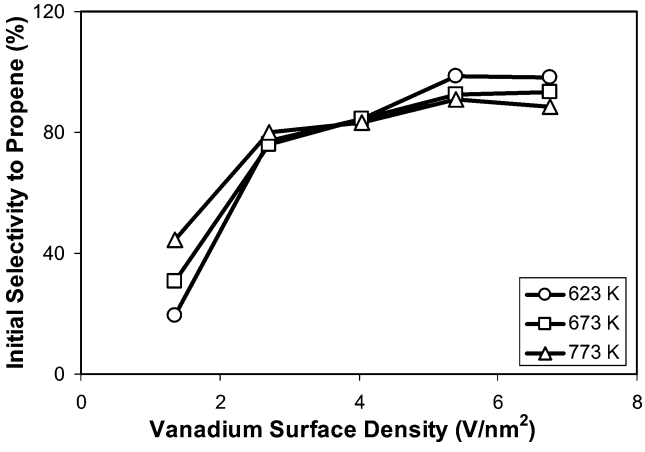

Fig. 9. Dependence of propene selectivities on the apparent vandia surface density and reaction temperature for the V/MgAl catalysts.

loadings less than 6 V/nm^2 can be attributed to the higher activity of polyvanadate domains relative to monovanadate species [2].

A plot of propene selectivity at zero propane conversion is shown in Fig. 9 as a function of vanadium surface density at three different temperatures. At 673 K the propene selectivity increases up to a vanadium surface density of ~ 6 V/nm^2, after which it remains constant at 98%. Increasing the reaction temperature resulted in a slight decrease in propene selectivity. The observed trend in propene selectivity with increasing vanadium surface density is very similar to that reported for vanadia dispersed on MgO, Al_2O_3, Scheme 1 and ZrO_2 [1,2,7].

Further insight into the catalytic properties of the V/MgAl catalysts can be obtained from an analysis of the rate data on the basis of Scheme 1. It has been shown that a propane/oxygen mixture can react via parallel and sequential steps. At low oxygen conversions, the rate coefficients for the oxidative dehydrogenation, k_1, primary combustion

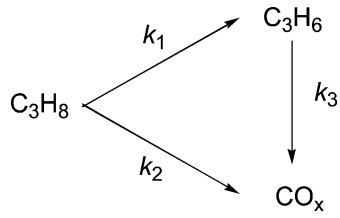

Scheme 1.

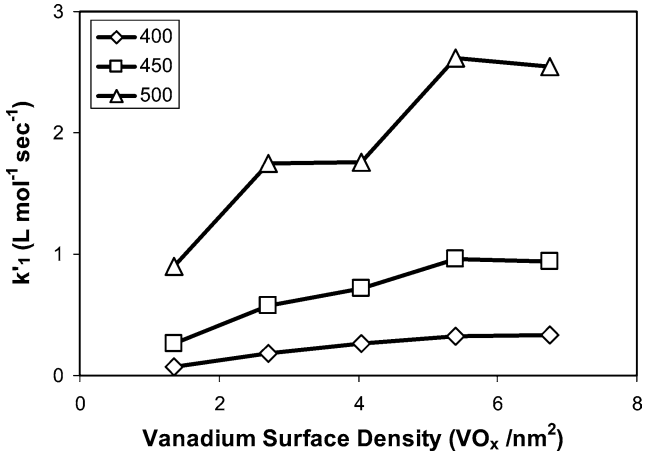

Fig. 10. Dependence of k_1 on the apparent vanadium surface density and reaction temperature for the V/MgAl catalysts.

of propane, k_2, and secondary combustion of propene, k_3, can be readily obtained from the experimental data. The derivation of this kinetic analysis is detailed elsewhere [8,9].

The values of k_1 as a function of vanadium surface density for temperatures of 673, 723, and 773 K are shown in Fig. 10. At all three temperatures the value of k_1 reaches a maximum value at vanadium surface density of ~ 5 V/nm^2. For higher surface densities, the value of k_1 approaches a plateau. This trend can be explained in terms of changes in the structure of the dispersed vanadia with increasing vanadium surface density. At low surface densities (below 5 V/nm^2), vanadia is present primarily as isolated monovanadate species as demonstrated by Raman and ^{51}V SS-NMR spectroscopy. An increase in vanadium surface density, leads to the formation of more active tetrahedral polyvanadate species. Exceeding a weight loading of ~ 6 V/nm^2, a value consistent with the formation of a theoretical vanadia monolayer, causes the k_1 values to plateau.

The activation energy for propane ODH (E_1), propane combustion (E_2), and propene combustion (E_3), obtained from plots of $\ln k_1$ versus $1/T$, is shown in Fig. 11 as a function of vanadium weight loading. The activation energy for propane ODH decreases from 111 kJ/mol as the vanadium surface density increases and reaches a plateau at about 90 kJ/mol for surface densities > 6 V/nm^2. The activation energy for propane combustion increases from 58 kJ/mol at the lowest surface density until it reaches a maximum at 182 kJ/mol at a surface density of ~ 6 V/nm^2. The decreased activation energies at lower surface densities suggest

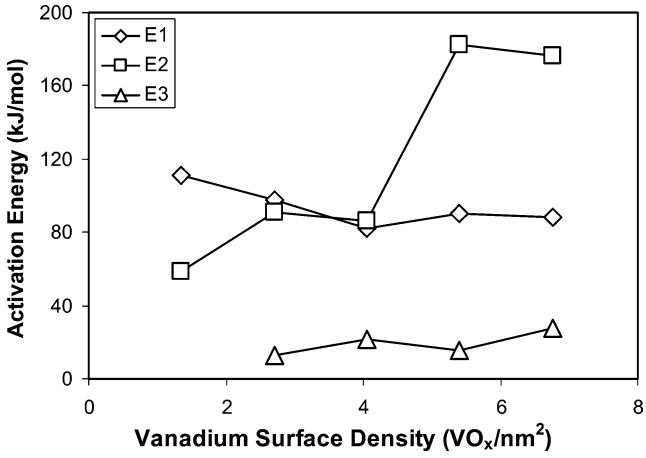

Fig. 11. Activation energies for propane ODH, E_1, propane combustion, E_2, and propene combustion, E_3, as a function of vanadium weight loading.

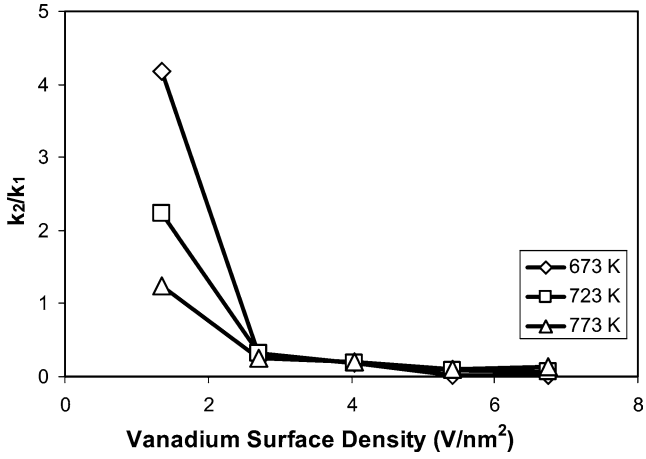

Fig. 12. Dependence of k_2/k_1 on the apparent vanadium surface density and reaction temperature for the V/MgAl catalysts.

that the $MgAl_2O_4$ support is active in propane combustion. The activation energy for propene combustion, on the one hand, seems to be independent of vanadium surface density and ranges from 16 to 26 kJ/mol.

The effects of vanadium surface density on k_2/k_1 are shown in Fig. 12. The values of k_2/k_1 decrease rapidly with increasing vanadium surface density. These values approach zero at a vanadium surface density of ~ 5 V/nm^2 and suggest that the rate of propane combustion becomes negligible in comparison to the rate of propane ODH as more VO_x species react with less selective sites on the support surface.

A plot of k_3/k_1 as a function of vanadium surface density is shown in Fig. 13. The value of k_3/k_1 decreases significantly with increasing vanadium surface density; however, this trend becomes less pronounced as the temperature increases. At all temperatures there is little effect of vanadium surface density on k_3/k_1 for densities greater than ~ 4 V/nm^2. At all surface densities the value of k_3/k_1 decreases with increasing temperature, indicating that the activation energy for propene combustion (E_3) is lower than that for propane ODH (E_1).

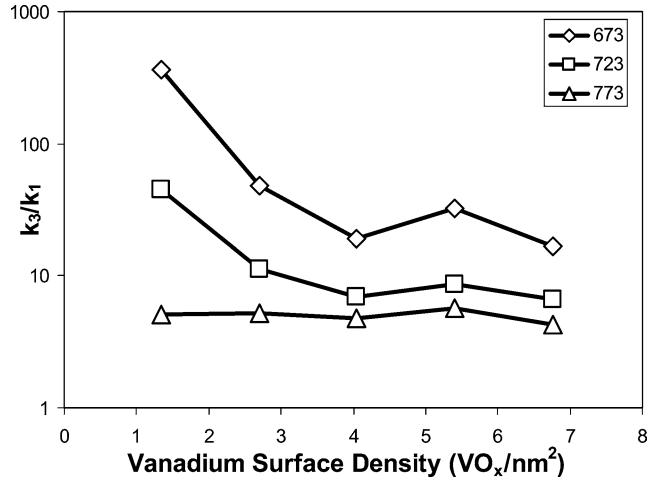

Fig. 13. Dependence of k_3/k_1 on the apparent vanadium surface density and reaction temperature for the V/MgAl catalysts.

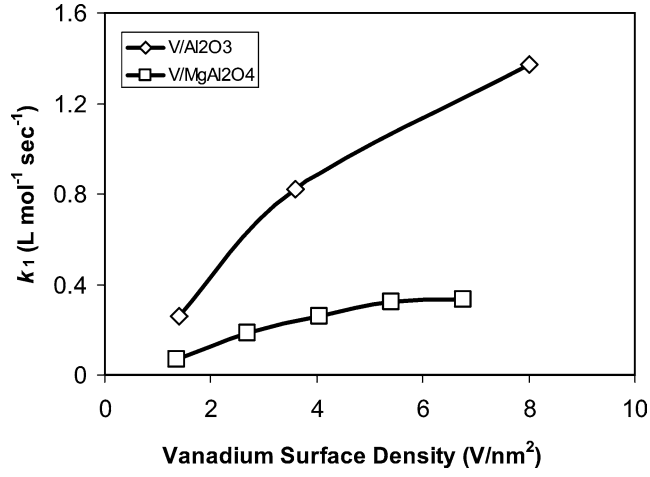

Fig. 14. Comparison of the k_1 values obtained for V/MgAl and VO_x/Al_2O_3 catalysts. Reaction conditions for V/MgAl and (for VO_x/Al_2O_3): temperature, 673 K (663 K); feed flow rate, C_3H_8/He/O_2 at 25/200/9 (34/215/4) cm^3/min.

3.3. Comparison of catalysts

It is interesting to compare the V/MgAl catalysts reported in this study to V/Al_2O_3 catalysts previously reported [2]. A comparison to previously reported V/MgO catalysts cannot be made because the active VO_x species in these catalysts exist as dispersed magnesium orthovanadate domains and differ markedly in the structure and reactivity from the VO_x species observed on V/MgAl and V/Al_2O_3 catalysts. Fig. 14 shows that the values of k_1 obtained for the V/Al_2O_3 are considerably larger than the V/MgAl catalysts. For both catalysts the values of k_1 increase with increasing vanadium surface density. Similar to the V/MgAl catalysts reported here, the VO_x surface species on V_2O_5/Al_2O_3 catalysts at low weight loadings exist mainly as isolated monovanadate species. The gradual increases in k_1 values with increasing vanadium surface density suggest that tetrahedral polyvanadate species are more active in propane ODH than isolated

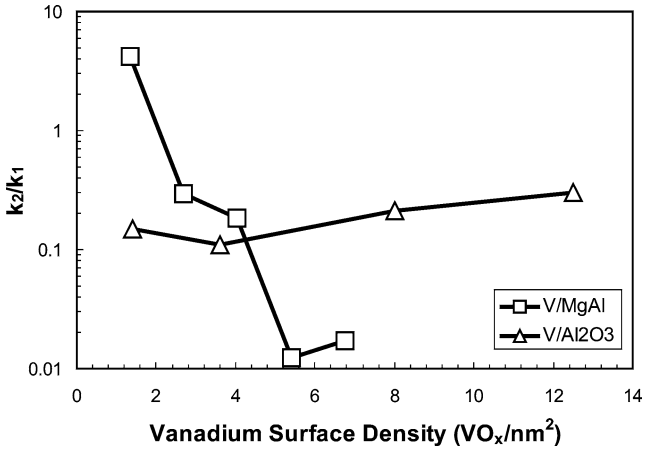

Fig. 15. Comparison of the k_2/k_1 values obtained for V/MgAl and VO_x/Al_2O_3 catalysts. Reaction conditions for V/MgAl and (for VO_x/Al_2O_3): temperature, 673 K (663 K); feed flow rate, C_3H_8/He/O_2 at 25/200/9 (34/215/4) cm^3/min.

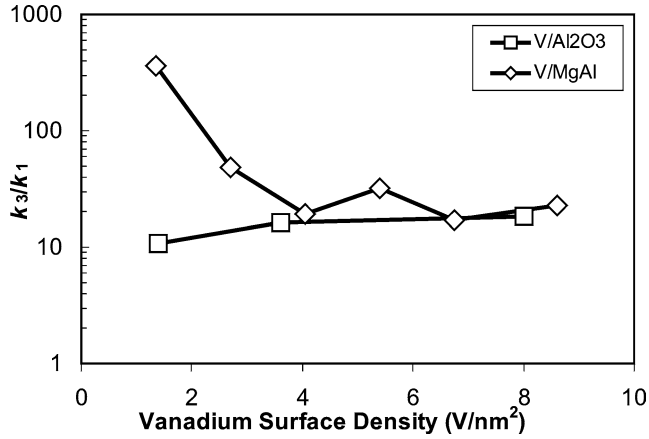

Fig. 16. Comparison of the k_3/k_1 values obtained for V/MgAl and VO_x/Al_2O_3 catalysts. Reaction conditions for V/MgAl and (for VO_x/Al_2O_3): temperature, 673 K (663 K); feed flow rate, C_3H_8/He/O_2 at 25/200/9 (34/215/4) cm^3/min.

monovanadate species. The larger k_1 values obtained for the V/Al_2O_3 catalysts can be ascribed to the formation of a two-dimensional VO_x monolayer which has been shown to be more active than the smaller and more disperse polyvanadate species observed on the V/MgAl catalysts reported here.

Fig. 15 shows the ratios of rate coefficients for alkane combustion and dehydrogenation (k_2/k_1) as a function of vanadium surface density for both catalysts. The k_2/k_1 values for V_2O_5/Al_2O_3 catalysts increase slightly with increasing vanadium surface density. It has been reported that isolated monovanadate species supported on Al_2O_3 are considerably more selective than polyvanadate species. The slight increase in k_2/k_1 values for these catalysts can thus be ascribed to a decrease in initial propene selectivities owing to the formation of bulk polyvanadate species at increased vanadium surface density. On the other hand, the k_2/k_1 values obtained for the catalysts reported in this study show the opposite trend and decrease rapidly with increasing vanadium surface density, reaching a plateau at ~ 4 V/nm^2. The high values of k_2/k_1 at low weight loadings reflect poor initial propene selectivities and suggest that the bare $MgAl_2O_4$ support efficiently catalyzes the direct combustion of propane. Upon grafting of the vanadium precursor, the sites responsible for alkane combustion are blocked resulting in the observed decrease in k_2/k_1 values. At a vanadium surface density of greater than ~ 4 V/nm^2 the V/MgAl catalysts exhibit lower k_2/k_1 values than those obtained for the V_2O_5/Al_2O_3 catalysts. This suggests that the V/MgAl catalysts exhibit a lower relative reactivity for the combustion of propane.

A plot of k_3/k_1 with respect to vanadium surface density is shown in Fig. 16 for both V/MgAl and V_2O_5/Al_2O_3 catalysts. The data obtained for V_2O_5/Al_2O_3 display a modest increase in k_3/k_1 values with increasing vanadium surface density. On the other hand, the values obtained for V/MgAl catalysts initially decrease at low weight loadings and then plateau at a vanadium surface density of ~ 4 V/nm^2. This behavior seems to suggest that the bare $MgAl_2O_4$ support, which is somewhat active in alkane combustion, is also active in alkene combustion. At higher weight loadings, the k_3/k_1 values obtained for the V/MgAl catalysts approach those obtained for the V_2O_5/Al_2O_3 catalysts. The lower k_1 values obtained for the V/MgAl catalysts suggest that these catalysts must have k_3 values considerably better than the V_2O_5/Al_2O_3 catalysts. The V/MgAl catalysts thus exhibit a lower relative reactivity toward the combustion of propene as compared to the V_2O_5/Al_2O_3 catalysts. This behavior is likely a direct result of the increase in basicity of the $MgAl_2O_4$ support. It has been previously reported that $MgAl_2O_4$ possesses acid and base sites intermediate in strength relative to MgO and Al_2O_3 [34–36]. It can thus be concluded that the incorporation of Mg into the catalyst support results in a decrease in the rate of propene combustion via an increase in the relative basicity of the catalyst support. The increase in basicity likely reduces alkene adsorption and provides for a rapid desorption of the propene product prior to secondary combustion.

4. Conclusions

A series of vanadia-based catalysts supported on a high-surface-area $MgAl_2O_4$ support were prepared via the non-aqueous grafting of a $OV(O^tBu)_3$ molecular precursor. After calcination at 823 K, the V/MgAl catalysts have BET surface areas of 234–245 m^2/g. Structural characterizations suggest that at all vanadium weight loadings tetrahedral monovanadate and polyvanadate species are the dominant surface species in the V/MgAl catalysts. According to SS ^{51}V NMR, Raman, and DRUV–vis spectroscopy, an increase in the weight loading on these catalysts results in an increase in the ratio of tetrahedral polyvanadate surface species to isolated monovanadates. A weight loading above the value corresponding to the formation of a theoretical polyvana-

date monolayer results in the formation of a small amount of octahedral vanadium species. Raman and DRUV–vis spectroscopy suggest that the V/MgAl catalysts appear to have an increased dispersion of VO_x species in comparison to V/Al_2O_3 catalysts at the same weight loadings. At low propane conversions, the V/MgAl catalysts are highly selective and active propane ODH catalysts. Owing to a high dispersion of VO_x species and a large population of more active tetrahedral polyvanadate species, the V/MgAl catalysts possess moderate activities (per vanadium atom). The V/MgAl catalysts are less active and more selective than previously reported V/Al_2O_3 catalysts. The diminished activities obtained for the V/MgAl catalysts are likely due to an increased VO_x dispersion and the formation of smaller polyvanadate domains as evidenced by Raman, DR–UV–vis, and SS-NMR spectroscopy. Analysis of the catalytic and spectroscopic data suggests that tetrahedral polyvanadate species are the most active species in propane oxidative dehydrogenation.

Acknowledgments

The authors acknowledge Mr. R.L. Brutchey for assistance in acquiring TEM micrographs. This work was supported by the Director, Office of Basic Energy Sciences, Chemical Sciences Division of the US Department of Energy under Contract DE-AC03-76SF00098.

References

[1] C. Pak, A.T. Bell, T.D. Tilley, J. Catal. 206 (2002) 49.
[2] M.D. Argyle, K. Chen, A.T. Bell, E. Iglesia, J. Catal. 208 (2002) 139.
[3] M.A. Chaar, D. Patel, H.H. Kung, J. Catal. 109 (1988) 463.
[4] D. Siew Hew Sam, V. Soenen, J.C. Volta, J. Catal. 123 (1990) 417.
[5] A. Corma, J.M. Lopez-Nieto, N. Paredes, M. Perez, Y. Shen, H. Cao, S.L. Suib, Stud. Surf. Sci. Catal. 72 (1992) 213.
[6] J.G. Eon, R. Olier, J.C. Volta, J. Catal. 145 (1994) 318.
[7] J.L. Male, H.G. Niessen, A.T. Bell, T.D. Tilley, J. Catal. 194 (2000) 431.
[8] A. Khodakov, B. Olthof, A.T. Bell, E. Iglesia, J. Catal. 181 (1999) 205.
[9] A. Khodakov, J. Yang, S. Su, E. Iglesia, A.T. Bell, J. Catal. 177 (1998) 343.
[10] M. Puglisi, F. Arena, F. Frusteri, V. Sokolovskii, A. Parmaliana, Catal. Lett. 41 (1996) 41.
[11] R. Grabowski, B. Grzybowska, K. Wcislo, Pol. J. Chem. 68 (1994) 1803.
[12] B. Grzybowska, I. Gressel, K. Samson, K. Wcislo, J. Stoch, M. Mikolajczyk, F. Dautzenberg, Pol. J. Chem. 75 (2001) 1513.
[13] M. Machli, E. Heracleous, A.A. Lemonidou, Appl. Catal. A 236 (2002) 23.
[14] F. Arena, F. Frusteri, A. Parmaliana, G. Martra, S. Coluccia, Stud. Surf. Sci. Catal. 119 (1998) 665.
[15] P. Concepcion, A. Galli, J.M. Lopez Nieto, A. Dejoz, M.I. Vazquez, Top. Catal. 3 (1996) 451.
[16] A.A. Lemonidou, L. Nalbandian, I.A. Vasalos, Catal. Today 61 (2000) 333.
[17] F. Arena, F. Frusteri, A. Parmaliana, Catal. Lett. 60 (1999) 59.
[18] C.K. Narula, US Patent No. 5,403,807 (1995).
[19] W. Prandtl, L.Z. Hess, Z. Anorg. Allg. Chem. 82 (1913) 103.
[20] G. Deo, I.E. Wachs, J. Haber, Crit. Rev. Surf. Chem. 4 (1994) 141.
[21] S.T. Oyama, G.T. Went, K.B. Lewis, A.T. Bell, G.A. Somorjai, J. Phys. Chem. B 93 (1989) 6786.
[22] B. Olthof, A. Khodakov, A.T. Bell, E. Iglesia, J. Phys. Chem. B 104 (2000) 1516.
[23] I.E. Wachs, Catal. Today 27 (1996) 437.
[24] M.A. Vuurman, I.E. Wachs, J. Phys. Chem. 96 (1992) 5008.
[25] D. Bersani, G. Antonioli, P.P. Lottici, T. Lopez, J. Non-Cryst. Solids 232–234 (1998) 175.
[26] H. Richter, Z.P. Wang, L. Ley, Solid State Commun. 39 (1981) 625.
[27] L.R. Le Coustumer, B. Taouk, M. Le Meur, E. Payen, M. Guelton, J. Grimblot, J. Phys. Chem. B 92 (1988) 1230.
[28] J. Tauc, in: J. Tauc (Ed.), Amorphous and Liquid Semiconductors, Plenum, London, 1974.
[29] E. Iglesia, D.G. Barton, S.L. Soled, S. Miseo, J.E. Baumgartner, W.E. Gates, G.A. Fuentes, G.D. Meitzner, Stud. Surf. Sci. Catal. 101 (1996) 533.
[30] K. Chen, A.T. Bell, E. Iglesia, J. Phys. Chem. B 104 (2000) 1292.
[31] R. Grabowski, B. Grzybowska, K. Samson, J. Sski, J. Stoch, K. Wciso, Appl. Catal. A 125 (1995) 129.
[32] A. Corma, J.M. López-Nieto, N. Paredes, M. Pérez, Appl. Catal. A 97 (1993) 159.
[33] P. Viparelli, P. Ciambelli, L. Lisi, G. Ruoppolo, G. Russo, J.C. Volta, Appl. Catal. A 184 (1999) 291.
[34] J.A. Lercher, React. Kinet. Catal. Lett. 20 (1982) 409.
[35] J.A. Lercher, React. Kinet. Catal. Lett. 23 (1983) 365.
[36] J.A. Lercher, J. Chem. Soc., Faraday Trans. 1 80 (1984) 949.